miR-129-5p regulates HMGB1/RAGE axis to inhibit pyroptosis and ameliorate cervical epithelial cell deterioration

Huafang Wang, Dilidaer Sidike, Pan Liu, Longge Suo, Huerxidan Niyazi

First Department of Oncology Center, The First Affiliated Hospital of Xinjiang Medical University, Urumqi, China

ABSTRACT

Cervical cancer is a serious gynecological malignancy, and the specific mechanisms of miR-129-5p remain unclear. This study aims to investigate the mechanism by which miR-129-5p regulates the high mobility group box 1 (HMGB1/receptor for advanced glycation end-products (RAGE) axis to inhibit pyroptosis and ameliorate cervical epithelial cell deterioration. Using RT-qPCR and Western blotting, we detected significantly downregulated miR-129-5p and upregulated HMGB1 in cervical cancer cells. To establish a deterioration model, we stimulated cervical epithelial cells with lipopolysaccharide (LPS). Further results revealed that miR-129-5p overexpression markedly reduced HMGB1 expression, suppressed RAGE activation, and decreased pyroptosis executer GSDMD-N production. Additionally, we conducted miR-129-5p overexpression and knockdown experiments to verify its regulatory effects on the HMGB1/RAGE axis and downstream pathways. Caspase-1 activity assays confirmed reduced pyroptosis upon miR-129-5p overexpression. Cell viability and proliferation were assessed using EdU incorporation assays and colony formation experiments. Our data demonstrated significant downregulation of miR-129-5p in cervical cancer cells. Overexpression of miR-129-5p substantially reduced HMGB1 expression and inhibited RAGE activation, thereby decreasing production of the pyroptosis executer GSDMD-N. LPS stimulation potently activated the HMGB1/RAGE axis and induced pyroptosis, while miR-129-5p overexpression inhibited these processes and ameliorated *in vitro* cervical epithelial cell deterioration. Cells overexpressing miR-129-5p exhibited attenuated caspase-1 activity with enhanced survival and proliferation following LPS treatment. Collectively, these *in vitro* findings indicate that miR-129-5p suppresses HMGB1/RAGE-mediated pyroptosis and cellular deterioration and also provide new mechanistic insights for cervical cancer therapeutics.

Key words: miR-129-5p; HMGB1/RAGE axis; pyroptosis; cervical cancer; LPS.

Correspondence: Huerxidan·Niyazi. First Department of Oncology Center, The First Affiliated Hospital of Xinjiang Medical University, No. 137 Liyushan South Road, Xinshi District, Urumqi, Xinjiang 830000, China.
E-mail: wanghuafang1215@126.com

Contributions: HW, conceptualization, investigation, methodology, data curation, manuscript original drafting; DS, PL, conceptualization, methodology, formal analysis, manuscript original drafting; LS, conceptualization, methodology, manuscript original drafting and reviewing; HN, supervision, methodology, investigation, conceptualization, data curation, formal analysis, funding acquisition, manuscript original drafting and reviewing. All authors read and approved the final version of the manuscript and agreed to be accountable for all aspects of the work.

Conflict of interest: the authors declare no competing interests, and all authors confirm accuracy.

Ethics approval: not applicable.

Funding: this study was supported by Project of Provincial-Ministry Joint Establishment of State Key Laboratory of Causes and Prevention of High Morbidity in Central Asia (No. SKL-HIDCA-2023-37).

Availability of data and materials: the datasets generated during and/or analyzed during the current study are available from the corresponding author on reasonable request.

Introduction

Cervical cancer (CC) is primarily caused by the persistent infection of human papillomavirus (HPV), leading to the deterioration of cervical epithelial cells.[1] Currently, the most effective way to prevent CC is through HPV vaccination. However, in some resource-limited regions, low vaccination coverage and limited awareness of CC prevention often led to delayed diagnosis and advanced-stage disease.[2] According to the World Health Organization (WHO), CC remains the fourth most common cancer among women worldwide. In 2020, there were 604,000 new cases, and among the 342,000 deaths caused by CC, approximately 90% occurred in low- and middle-income countries. Therefore, elucidating the mechanisms of cervical epithelial cell deterioration is of significant importance for the treatment of CC.

MicroRNAs (miRNAs) are a class of evolutionarily conserved non-coding small RNAs, typically 21-23 nucleotides in length, that regulate gene expression at the translational level.[3] Since their discovery, miRNAs have been reported to be involved in the pathogenesis of various diseases, such as cardiovascular diseases, cancer, kidney diseases, and diabetes.[4-7] In CC, miRNAs have also been observed to exhibit differential expression, and several miRNAs have been identified as biomarkers for CC.[8] Among them, miR-129-5p is significantly downregulated in CC. Targeting miR-129-5p delivers dual clinical-translational value as an early-detection biomarker and CRISPR-Cas9-modulatable therapeutic target, directly addressing CC management gaps in underserved populations. A study found that upregulating miR-129-5p decreased ZIC2, Shh, Gli1, Gli2, Chemokine ligand 1, VEGF, and Ang2 levels, inhibiting angiogenesis, migration, and invasion in CC cells. Similarly, nude mice showed inhibited tumor growth and angiogenesis.[9] The explanation of these two opposite conclusions may be explained by the fact that miR-129-5p plays different roles in each stage of CC development; therefore, its underlying mechanism requires further study.[10] Studies have shown that miR-129-5p can inhibit the proliferation of gastric cancer cells by targeting and suppressing the expression of high mobility group box 1 (HMGB1).[11] The HMGB1 is a DNA-bound nuclear protein which is actively released after cytokine stimulation and passively released after the death of these cells.[12] The receptor for advanced glycation end-products (RAGE) is a receptor with many ligands that binds molecules of diverse structures.[13] Additionally, studies have shown that isoflurane can regulate pyroptosis *via* the HMGB1/RAGE axis, affecting cancer progression in lung cancer.[14] In CC, it has been found that inhibition of the HMGB1/RAGE axis suppresses lipopolysaccharide (LPS)-induced malignant transformation of cervical epithelial cells, accompanied by the involvement of pyroptosis.[15] However, the interplay between miR-129-5p, the HMGB1/RAGE axis, and pyroptosis in the pathogenesis of CC has not been elucidated.

Based on this, we hypothesize that miR-129-5p regulates the HMGB1/RAGE axis to inhibit pyroptosis and ameliorate cervical epithelial cell deterioration during the development of CC. To test this hypothesis, we used cervical epithelial cells as a model, treated them with LPS to simulate the deteriorative environment *in vitro*, and performed overexpression/knockdown of miR-129-5p combined with RAGE inhibitors. We measured pyroptosis markers, cell migration and proliferation, and inflammatory factors to reveal the role of miR-129-5p in the pathogenesis of CC, aiming to further elucidate the mechanisms underlying CC development.

Materials and Methods

Experimental instruments

The experimental materials included cell culture flasks T25 (TCF012050), T75 (TCF012250), 6-well plates (TCP011006), 15 mL centrifuge tubes (CFT920150), and 50 mL centrifuge tubes (CFT920500) from Jet BIOFIL, Guangzhou, China; nuclease-free pipette tips from KeyGEN, Nanjing China; 1.5 mL nuclease-free centrifuge tubes (MCT-150-C) from Axygen, Beijing, China; pipettes, nitrile latex gloves; 0.2 mL PCR single tubes (PCR-02-C); 0.1 mL qPCR eight-tube strips (TLS0851) from Bio-Rad, Hercules, CA, USA; fluorescent quantitative 96-well PCR plates (F603102), fluorescent quantitative nuclease-free sealing films (F604419) from Sangon, Shanghai, China; PVDF membranes (IPVH00010) from Sigma-Aldrich, St. Louis, MO, USA; electrophoresis tank glass plate thin plates (1653308) and thick plates (1653311) from Bio-Rad.

Experimental reagents

Fetal bovine serum (FSD500) (Excell Bio, Suzhou, China); penicillin-streptomycin solution (100×) (C0222) (Beyotime, Shanghai, China); complete medium for human cervical epithelial cells (CM-H059) (Pricella, Beijing, China); trypsin (R001100) (Gibco, Shanghai, China); cell freezing medium (C0210B-50mL), PBS buffer (C0221A) (Beyotime); cell/tissue total RNA isolation kit V2 (RC112), HiScript III 1st strand cDNA synthesis kit (R312), Taq Pro Universal SYBR qPCR master mix (Q712) (Vazyme, Nanjing, China); primers and their NC from Guangzhou RiboBio Co., Ltd. (Guangzhou, China); APS (ST005), RIPA (P0013B), PMSF (ST506), TEMED (ST728) (Beyotime); 30% Acr/Bic (BL513A), Tris-Base (BS083), TBS buffer powder (BL602A), BSA protein standard (BL673A), Tween-20 (BS100) (Biosharp, Wuhan, China); SDS (3250), glycine (1275), skim milk (1172) (BioFroxx, Beijing, China); BCA protein assay kit (WB6501), 5× SDS-PAGE loading buffer (WB2001), ECL substrate AB solution (P2100) (NCM Biotech, Suzhou, China); methanol (HB05) (Guangzhou Chemical Reagent, Guangzhou, China); annexin V-FITC apoptosis detection kit (C1062L) (Beyotime); 4% paraformaldehyde (P0099) (Beyotime); 1% crystal violet (V5265-250mL) (Sigma-Aldrich); dual-luciferase reporter assay kit (RG027) (Beyotime); Prestained protein marker II (10-200 kDa) (G2058-250UL, Servicebio, Beijing China); HiMark™ Prestained protein standard (LC5699) (Thermo Fisher, Waltham, MA, USA); recombinant anti-Ki-67 antibody [EPR3610] (ab92742), recombinant anti-RAGE antibody [EPR21171] (ab216329), anti-GSDMD antibody (ab155233) (Abcam, Cambridge, MA, USA); HMGB1 antibody #3935, caspase-1 (E9R2D) rabbit mAb #83383, NOD-, LRR- and pyrin domain-containing protein 3 (NLRP3) (D4D8T) rabbit mAb #15101, cleaved caspase-1 (Asp297) (D57A2) rabbit mAb #4199 (Cell Signaling Technology, Danvers, MA, USA); Western antibody GAPDH-loading control (bsm-33033M) (Bioss, Wuhan, China).

Cell culture

The cervical epithelial cells (CM-H059) were obtained from Procell Life Science & Technology Co. Ltd. (Wuhan, China). Cells were cultured in complete medium for human cervical epithelial cells. When the cell confluence reached 80%-90%, the culture medium was discarded, and the cells were washed twice with 2 mL PBS. Following removal of PBS, 2 mL of 0.25% trypsin-0.02% EDTA solution was added for digestion. Under microscopic observation, once the cells became rounded (approximately 1 min), digestion was promptly terminated by adding 6 mL of complete

medium. The cell suspension was gently pipetted to ensure homogeneity and then transferred to a sterile tube. Cells were centrifuged at 800 rpm for 5 min at 4°C, after which the supernatant was discarded. The cell pellet was resuspended in fresh complete medium and either sub-cultured or seeded at appropriate densities according to experimental requirements.

Experimental groups

The specific groups for LPS-induced deterioration of CM-H059[15] are shown in Table 1. The specific groups for the regulatory effect of miR-129-5p on HMGB1/RAGE were summarized in Table 2. miR-129-5p was found to the HMGB1/RAGE axis to inhibit cellular pyroptosis and improve deterioration of cervical epithelial cells (Table 3).

CCK-8 cell viability assay

Cells in logarithmic growth phase were seeded at a density of 2,000 cells per well in a 96-well plate and incubated at 37°C under 5% CO_2 for 4-8 h until adherent. After cells adhered, different concentrations of CURNPs were added according to experimental groups, with each group having 6 replicate wells. Following a 24-h incubation period, cells were treated with 10 µL of CCK-8 solution per well, 2 h prior to the conclusion of the incubation, to assess cell proliferation. After completion of the incubation, the absorbance at 450 nm was measured using a microplate reader.

ELISA

Cells in the logarithmic growth phase were seeded at a density of 1 × 10^6 cells per well in 6-well plates. Following cell attachment, a 12-h serum starvation period was performed prior to treatment. Cells were then subjected to experimental conditions and cultured for 24 h at 37°C under 5% CO_2. Supernatants were collected and centrifuged at 1,000 × g for 20 min to remove cellular debris. For ELISA analysis, standard samples were prepared according to the manufacturer's instructions and loaded into a 96-well microplate. Fifty microliters (50 µL) of each standard or test sample were added to the designated wells. The plate was sealed and incubated at 37 °C for 30 min. Afterward, the plate was washed five times with the provided washing buffer. Next, 50 µL of enzyme-conjugated detection antibody was added to each well, followed by an additional 30-min incubation at 37°C.

Following another round of washing, 50 µL of chromogen substrate A and 50 µL of substrate B were added sequentially. The plate was incubated in the dark at 37 °C for 15 min to allow color development. The reaction was terminated by adding 50 µL of stop solution to each well. Absorbance (optical density) was measured at the appropriate wavelength as specified in the ELISA kit instructions, enabling quantitative analysis of target analytes in the cell culture supernatants.

Western blot

Total protein was extracted from cells in the logarithmic growth phase (1×10^6 cells per well in a 6-well plate) following treatment according to the respective experimental groups. After incubation, cells were washed with PBS and lysed using RIPA buffer supplemented with PMSF. The lysates were centrifuged to collect supernatants, which were then stored at –80°C until further use. Protein concentration was determined using the BCA protein

Table 1. Experimental grouping with lipopolysaccharide.

Grouping	Specific procedures
Control	The cells were maintained under standard culture conditions
0.1 µg/mL LPS	Treat cells with 0.1 µg/mL LPS for 24 h
0.5 µg/mL LPS	Treat cells with 0.5 µg/mL LPS for 24 h
1.0 µg/mL LPS	Treat cells with 1.0 µg/mL LPS for 24 h

LPS, lipopolysaccharide.

Table 2. Experimental grouping with miR-129-5p.

Grouping	Specific procedures
Control	The cells were maintained under standard culture conditions
miR-129-5p-NC mimics	Transfection with miR-129-5p-NC mimics vector
miR-129-5p mimics	Transfection with miR-129-5p mimics vector
miR-129-5p inhibitor	Transfection with miR-129-5p inhibitor vector

Table 3. Experimental grouping with HMGB1/RAGE.

Grouping	Specific procedures
Control	The cells were maintained under standard culture conditions
LPS	Treat cells with 0.5 µg/mL LPS for 24 h
LPS+miR-129-5p mimics	Transfect cells with miR-129-5p overexpression vector and treat with 0.5 µg/mL LPS for 24 h.
LPS+miR-129-5p NC mimics	Transfect cells with miR-129-5p-NC overexpression vector and treat with 0.5 µg/mL LPS for 24 h.
LPS+miR-129-5p mimics+OE-RAGE	Transfect cells simultaneously with miR-129-5p overexpression vector and RAGE vector, then treat with 0.5 µg/mL LPS for 24 h.

LPS, lipopolysaccharide.

assay kit. Equal amounts of protein were subjected to SDS-PAGE and subsequently transferred onto PVDF membranes. The membranes were blocked with 5% non-fat milk or BSA solution, depending on the antibody requirements, and incubated overnight at 4°C with primary antibodies diluted as specified in Table 4. Following primary incubation, membranes were washed and incubated with corresponding secondary antibodies for 2 h at room temperature. Protein bands were visualized using an enhanced chemiluminescence detection system (JP-K6000), and band intensities were quantified using ImageJ software. This completed the Western blot analysis procedure.

RT-qPCR

Total RNA was extracted from cervical epithelial cells in the logarithmic growth phase, seeded at a density of 1×10^6 cells per well in 6-well plates and treated according to the experimental groups for 24 h. Following treatment, cells were lysed with 500 µL of Buffer RL, and the lysate was transferred to FastPure gDNA Filer Columns III (Vazyme) for genomic DNA removal *via* centrifugation. The flow-through was mixed with an equal volume of 70% ethanol and loaded onto FastPure RNA Spin Columns III. RNA was purified through sequential washes with Buffer RW1 and RW2, followed by elution using RNase-free ddH_2O. RNA quantity and purity were assessed using a NanoDrop ND-2000 spectrophotometer (Thermo Fisher Scientific). Complementary DNA (cDNA) synthesis was performed using a 20 µL reaction system containing up to 1 µg of total RNA, 5× gDNA Wiper Mix, RNase-free water, 10× RT Mix, Hiscript III Enzyme Mix, Oligo(dT)20VN, and Random Hexamers, following the manufacturer's instructions (Vazyme). The reaction was carried out at 42°C for 15 min, followed by 85°C for 5 s. RTqPCR was conducted using a 20 µL reaction mixture containing diluted cDNA, nuclease-free water, 2× Taq Pro Universal SYBR qPCR Master Mix (Vazyme), and gene-specific forward and reverse primers. Amplification was performed on a CFX96 Touch Real-Time PCR Detection System (Bio-Rad) under the following conditions: initial denaturation at 95°C for 3 min, followed by 40 cycles of denaturation at 95°C for 10 s, annealing/extension at 60 °C for 30 ss, and a final melt curve analysis. Relative mRNA expression levels were normalized to GAPDH and calculated using the $2^{-\Delta\Delta Ct}$ method. Primer sequences used are listed in Table 5.

Fluorescence reporter assay

To validate the direct interaction between miR-129-5p and HMGB1, a luciferase reporter assay was performed. A miR-129-5p/HMGB1 dual-luciferase reporter vector was constructed based on the miR-129-5p binding sequence obtained from NCBI. The pmir-GLO Dual-Luciferase Vector (Promega) was utilized, which contains both firefly luciferase (FLuc) and Renilla luciferase (RLuc) reporter genes driven by the TK promoter. Wild-type and mutant forms of the HMGB1 3'UTR were synthesized and cloned into the vector. Plasmids were provided by Shanghai Sangon Biotech and divided into five groups: wild-type control, wild-type experimental, mutant control, mutant experimental, and internal control. Cells were co-transfected with plasmids at a ratio of 50:1 (reporter plasmid:microRNA mimic or negative control) using Lipofectamine 3000 reagent (Invitrogen) and incubated for 48 h.

Following transfection, cells were lysed and centrifuged to collect supernatants. Firefly and Renilla luciferase activities were measured using a GloMax Navigator Microplate Luminometer (Promega) according to the manufacturer's instructions. Relative luciferase activity was calculated as the ratio of firefly to Renilla luciferase luminescence (RLU). Mutation sites within the HMGB1 3'UTR are detailed in Table 6.

EdU assay for cell proliferation

Cells in logarithmic growth phase were seeded at 1×10^6 cells per well in a 6-well plate and treated according to experimental groups. A 2× EdU working solution (20 µM) was added to achieve a final concentration of 1× EdU, and cells were incubated for 2 h. After EdU labeling, cells were fixed with 4% paraformaldehyde for 15 min, washed three times with wash buffer, and permeabilized with 0.3% Triton X-100 in PBS for 15 min. Cells were washed again twice, and a Click Additive Solution was prepared and added to each well. The plate was gently shaken and incubated in the dark for 30 min, then washed three times. DAPI staining solution was added for 5 min, followed by three washes. Fluorescence was observed under a fluorescence microscope. EdU-stained cells were imaged using an Olympus IX73 inverted fluorescence microscope equipped with a 40× objective lens (NA 0.6). For each experimental group, 5 randomly selected fields per well (n=3 replicates) were analyzed. The EdU-positivity index was calculated as the percentage of EdU-positive cells (green fluorescence) relative to total DAPI nuclei (blue fluorescence) using ImageJ v1.53.

Scratch assay

In the scratch assay, cells in logarithmic growth phase were seeded at a density of 1×10^6 cells per well in a 6-well plate, according to their respective experimental groups. Parallel lines were marked 0.5 cm apart on the backside of the plate. Once cells reached over 90% confluency, scratches were created perpendicu-

Table 4. Antibody dilution ratios for Western blotting.

Antibodies	Dilution (application)
Ki-67	1:1000
HMGB1	1:1000
RAGE	1:1000
NLRP3	1:1000
caspase-1	1:1000
GSDMD	1:1000
cleaved caspase-1	1:1000
GAPDH	1:10000
Goat Anti-Rabbit IgG H&L(HRP)	1:20000
Goat Anti-Mouse IgG H&L(HRP)	1:20000

Table 5. Primer sequences for RT-qPCR.

Gene	Primer sequence (5' to 3')
miR-129-5p	Forward: GCGTTCGGGTCTGGCG Reverse: AGTGCAGGGTCCGAGGTATT
HMGB1	Forward: TCTCAGGGCCAAACCGATAG Reverse: TCGTGCACCGAAAGTTTCAA
RAGE	Forward: GCTTGGAAGGTCCTGTCTCC Reverse: CACGGACTCGGTAGTTGGAC
GAPDH	Forward: CGGGAAGGAAATGAATGGGC Reverse: GGAAAAGCATCACCCGGAGG

Table 6. Mutation sites for luciferase.

Mutation sites	
HMGB1 3' UTR	5'-GCAAAGCCUGAUGCAGCAAAAAA-3'
miR-129-5p	3'-CGUUCGGGUCUGGCGUUUUUC-5'
MUT HMGB1 3' UTR	5'-GCAAAGCCUGAUGCAAACGAAAA-3'

lar to the marked lines using a pipette tip. After washing twice with PBS, the initial (0-h) scratch width was photographed under a microscope. The plate was then incubated for 24 h, followed by washing and photographing again to record the scratch width at 24 h under the microscope. Scratch images were captured at 0 h and 24 h using a Nikon Eclipse Ts2 microscope (10×objective). Scratch width was quantified with NIS-Elements AR v5.21 software by measuring the distance between wound edges at three fixed positions per field. Data represent mean ± SD of three independent experiments.

Statistical analysis

The data were analyzed and plotted using GraphPad Prism 9 (Version 9.4.0; La Jolla, CA, USA). All data are presented as means ±SD. Statistical differences between groups were evaluated using either *t*-test or one-way ANOVA, with significance defined as $p<0.05$.

Results

LPS induced deterioration of cervical epithelial cells

As shown in Figure 1, compared to the untreated control cells (CK) group, the treatment of cervical epithelial cells with 0.1-1.0 μg/mL LPS for 24 h resulted in a significant decrease in cell viability (Figure 1, $p<0.001$), displaying a dose-dependent relationship within the tested concentration range. Simultaneously, the levels of IL-1β and IL-18 secreted by the cells also showed an increasing trend within the tested concentration range and were significantly different from those in the CK group (Figure 1, $p<0.001$). Taken together with previous reports, these results suggest that LPS can induce the deterioration of cervical epithelial cells, manifested as sustained pro-inflammatory milieu *via* IL-1β/IL-18 hypersecretion.

LPS regulated miR-129-5p, HMGB1/RAGE axis and pyroptosis

As shown in Figure 2, compared to the CK group, the treatment of cervical epithelial cells with 0.1-1.0 μg/mL LPS for 24 h resulted in a significant decrease in the expression level of miR-129-5p (Figure 2A, $p<0.001$). Simultaneously, the levels of Ki-67, HMGB1/RAGE axis components (HMGB1, RAGE), inflammasome sensors (NLRP3, caspase-1), and pyroptosis-related Gasdermin D (GSDMD) cleavage were significantly increased (Figure 2B, $p<0.001$). These results indicated that LPS regulates miR-129-5p, the HMGB1/RAGE axis, and pyroptosis, suggesting that LPS may induce the deterioration of cervical epithelial cells through these pathways.

miR-129-5p inhibited proliferation of cervical epithelial cells *via* the HMGB1/RAGE axis

As shown in Figure 3, compared to the CK group, knockdown of miR-129-5p in cervical epithelial cells led to increase expression levels of HMGB1 and RAGE, and significantly accelerate cell proliferation (Figure 3 A,C,D; $p<0.05$). This trend was reversed when miR-129-5p was overexpressed. Furthermore, the dual-luciferase reporter assay demonstrated a direct binding interaction between miR-129-5p and HMGB1 (Figure 3B). Combined with these experimental findings, the results indicated that miR-129-5p inhibited the proliferation of cervical epithelial cells *via* the HMGB1/RAGE axis.

miR-129-5p regulated HMGB1/RAGE axis to inhibit LPS-mediated pyroptosis

As shown in Figure 4, compared to the CK group, treatment with LPS resulted in a significant decrease in miR-129-5p expression, while elevating: HMGB1/RAGE axis components (HMGB1, RAGE), inflammasome sensors (NLRP3, caspase-1), and pyroptosis protein (GSDMD, cleaved caspase-1) (Figure 4A-B, $p<0.001$). Additionally, compared to the LPS group, overexpression of miR-129-5p significantly reduced the expression levels of HMGB1, RAGE, NLRP3, GSDMD, caspase-1, and cleaved caspase-1 ($p<0.01$). Notably, when RAGE was simultaneously overexpressed, this protective effect was substantially reversed ($p<0.01$), indicating RAGE's central role in mediating miR-129-5p's function. Taken together, these results indicate that miR-129-5p primarily suppresses LPS-induced pyroptosis by modulating the HMGB1/RAGE signaling axis, although additional regulatory factors may also contribute to its biological effects.

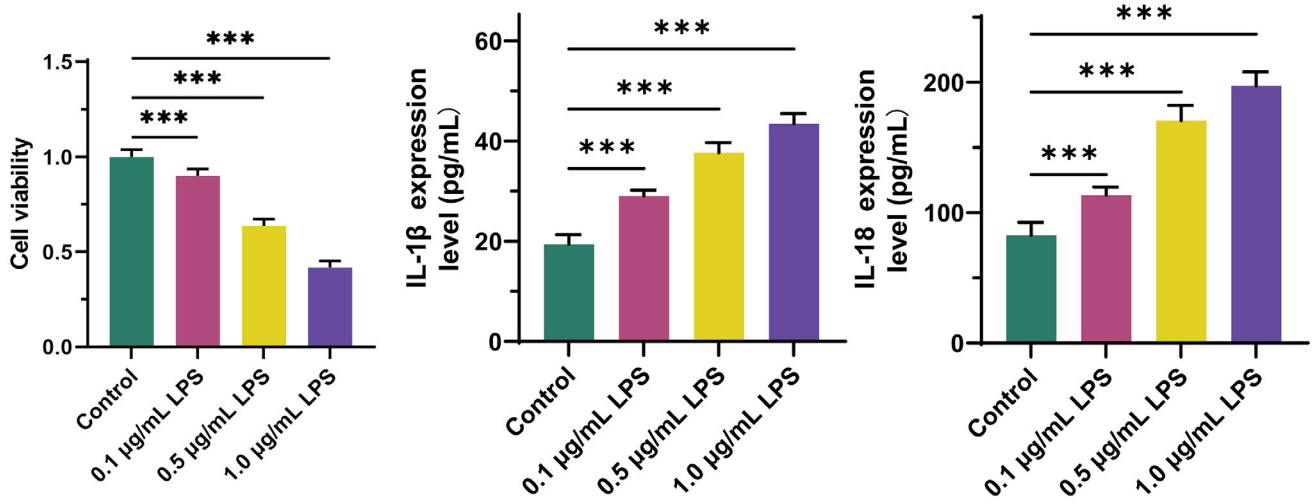

Figure 1. LPS induces cervical epithelial cell deterioration and proliferation. Cell viability was assessed using the CCK-8 assay following treatment with different concentrations of LPS (0, 1, 5, and 10 μg/mL) for 24 h. LPS treatment significantly enhanced cell viability in a dose-dependent manner. The levels of pro-inflammatory cytokines interleukin-1β (IL-1β) and interleukin-18 (IL-18) in the culture supernatants were measured by ELISA; LPS stimulation significantly increased the secretion of both IL-1β and IL-18. n=3, ***$p<0.001$.

miR-129-5p regulated HMGB1/RAGE axis to ameliorate LPS-mediated deterioration of cervical epithelial cells

As shown in Figure 5, compared to the CK group, treatment with LPS significantly enhanced the migration and proliferation abilities of cervical epithelial cells (Figure 5A-C, $p<0.001$), and increased the expression levels of IL-1β, IL-18, and TNF-α. Notably, these effects were significantly ameliorated when miR-129-5p was overexpressed ($p<0.01$). However, when RAGE was simultaneously overexpressed, this trend was reversed ($p<0.01$). *In vitro* data suggested miR-129-5p may regulates the HMGB1/RAGE axis to ameliorate LPS-mediated deterioration of cervical epithelial cells.

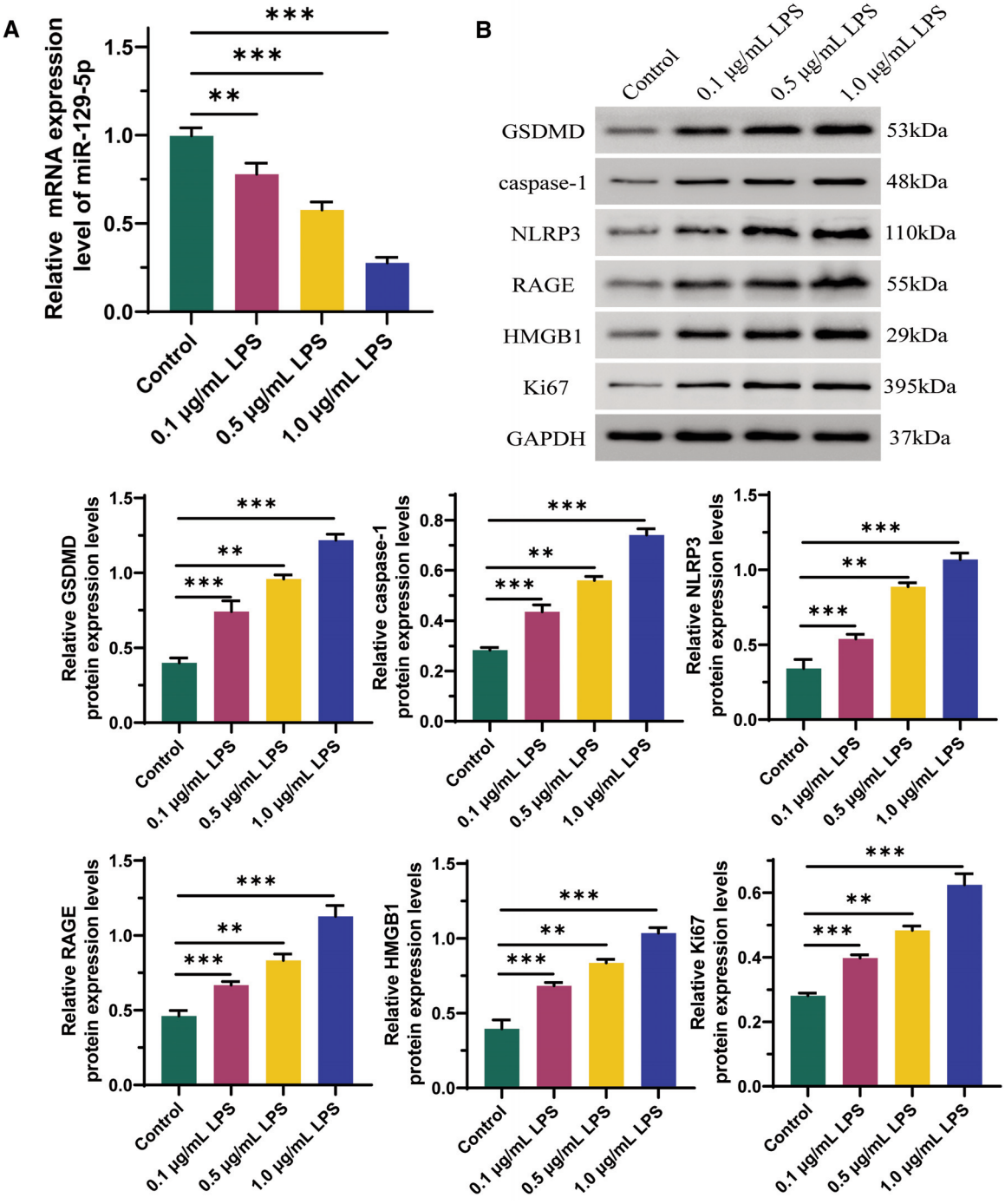

Figure 2. LPS regulates miR-129-5p, the HMGB1/RAGE axis, and pyroptosis. **A**) Quantitative real-time PCR was performed to evaluate the expression level of miR-129-5p in response to varying concentrations of LPS (0.1 μg/mL, 0.5 μg/mL, and 1.0 μg/mL) compared to a control group without LPS treatment. **B**) Western blot analysis was conducted to assess the expression levels of key components of the HMGB1/RAGE signaling axis (HMGB1, RAGE), proliferation (Ki-67) and pyroptosis-related proteins (NLRP3, caspase-1, and GSDMD); LPS treatment (0.1 μg/mL, 0.5 μg/mL, and 1.0 μg/mL) resulted in upregulation of HMGB1, RAGE, Ki-67 and pyroptosis-related proteins; β-actin served as the loading control. n=3, $^{**}p<0.01$, $^{***}p<0.001$.

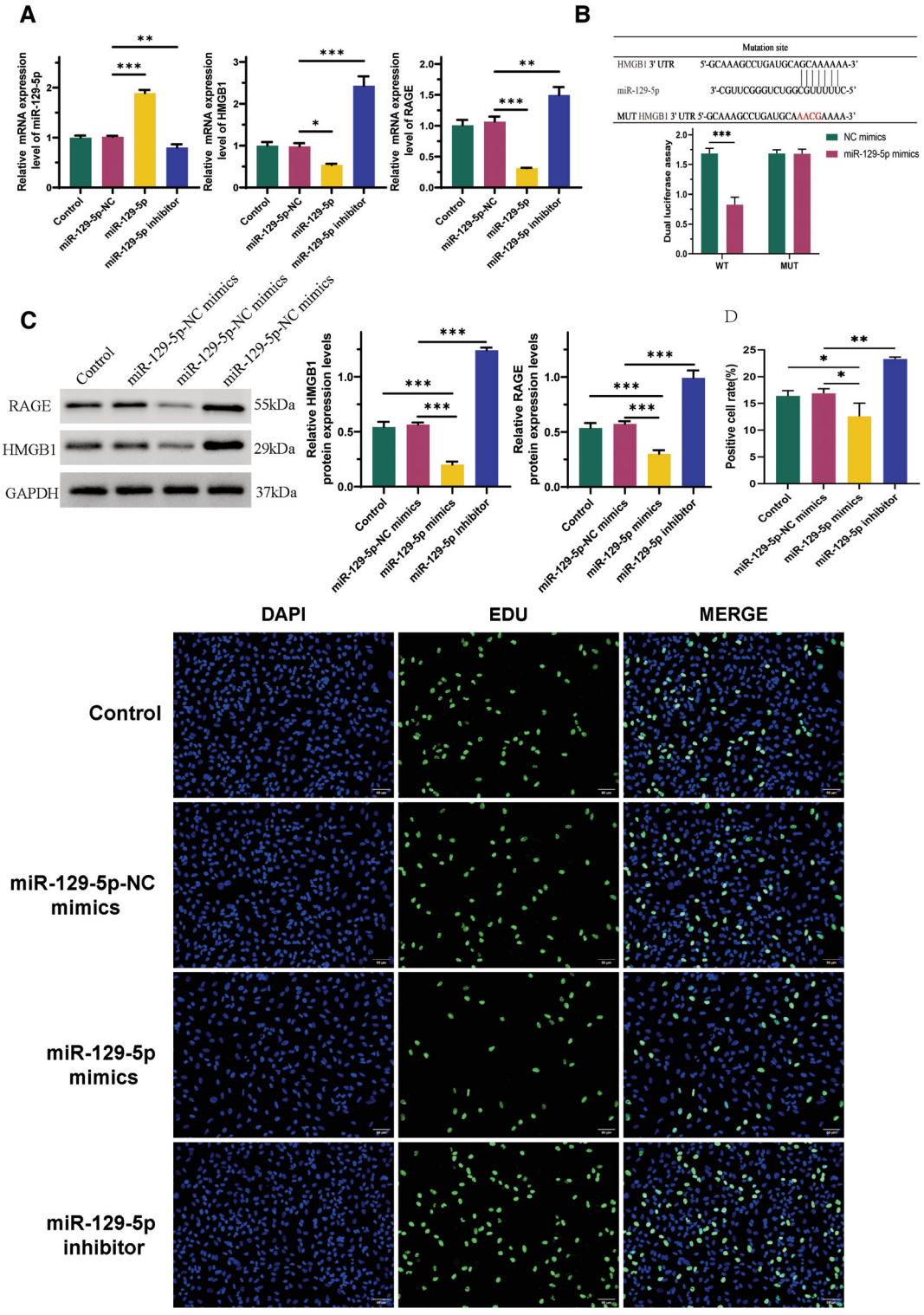

Figure 3. miR-129-5p inhibits the proliferation of cervical epithelial cells via the HMGB1/RAGE axis. **A**) RT-qPCR was used to measure the relative mRNA expression levels of miR-129-5p, HMGB1, and RAGE in cervical epithelial cells transfected with miR-129-5p mimics, miR-129-5p inhibitor, or their respective negative controls (NC). **B**) The dual-luciferase reporter assay was performed to confirm the direct targeting of HMGB1 by miR-129-5p; the 3' untranslated region (UTR) of HMGB1 containing the putative binding site for miR-129-5p was cloned into a luciferase reporter vector; co-transfection of miR-129-5p mimics with the wild-type (WT) HMGB1 3' UTR construct resulted in a significant decrease in luciferase activity, whereas no such effect was observed with the mutant (MUT) construct. **C**) Western blot analysis was conducted to evaluate the protein expression levels of HMGB1 and RAGE after transfection with miR-129-5p mimics, miR-129-5p inhibitor, or their respective NCs. GAPDH served as the loading control. **D**) Cell proliferation was assessed using the EdU incorporation assay; Transfection of miR-129-5p mimics significantly reduced the number of EdU-positive cells, indicating decreased cell proliferation; conversely, inhibition of miR-129-5p led to an increase in the number of EdU-positive cells, suggesting enhanced cell proliferation. Representative images are shown, and the positive cell rate (%) was quantified. n=3, *p<0.05, **p<0.01, ***p<0.001.

Discussion

miR-129-5p, an important non-coding small RNA, plays crucial regulatory roles in the development and progression of various cancers such as lung, ovarian, breast, and bladder cancers.[16-19] In CC, studies have shown significant downregulation of miR-129-5p, correlating closely with cancer progression and poor prognosis.[20] However, the specific mechanisms of miR-129-5p in CC remain incompletely understood. Current research has demonstrated that miR-129-5p played a significant role in regulating tumor cell proliferation, migration, and invasion.[21] Our findings

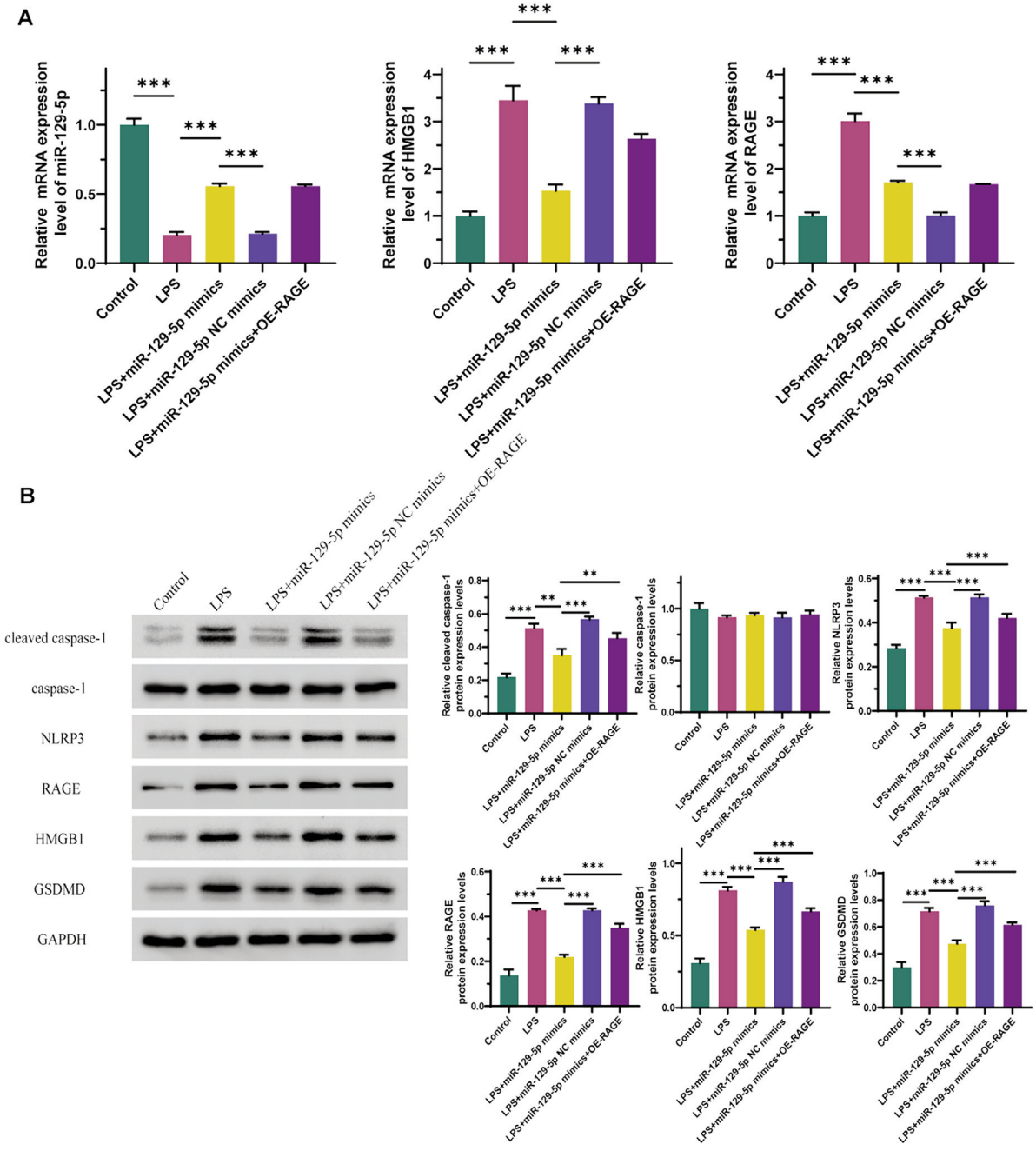

Figure 4. miR-129-5p regulates the HMGB1/RAGE axis to inhibit LPS-mediated pyroptosis. **A**) RT-PCR analysis revealed the relative mRNA expression levels of miR-129-5p, HMGB1, and RAGE in cervical epithelial cells under various treatment conditions, including untreated cells (Control), LPS treatment alone (LPS), LPS with miR-129-5p mimics (LPS+miR-129-5p mimics), LPS with miR-129-5p negative control mimics (LPS+miR-129-5p NC mimics), LPS with miR-129-5p inhibitor (LPS+miR-129-5p inhibitor), LPS with miR-129-5p negative control inhibitor (LPS+miR-129-5p NC inhibitor), and LPS with miR-129-5p mimics plus RAGE overexpression (LPS+miR-129-5p mimics + OE-RAGE); these results demonstrated that miR-129-5p modulated the HMGB1/RAGE axis and affected LPS-mediated pyroptosis. **B**) Western blot analysis was performed to assess the protein expression levels of key components in the HMGB1/RAGE axis (HMGB1, RAGE) and pyroptosis-related proteins (cleaved caspase-1, caspase-1, NLRP3, GSDMD) following LPS treatment and transfection with miR-129-5p mimics or their respective negative controls (NCs); additionally, RAGE overexpression constructs were co-transfected to evaluate their modulatory effects. n=3, $^{**}p<0.01$, $^{***}p<0.001$.

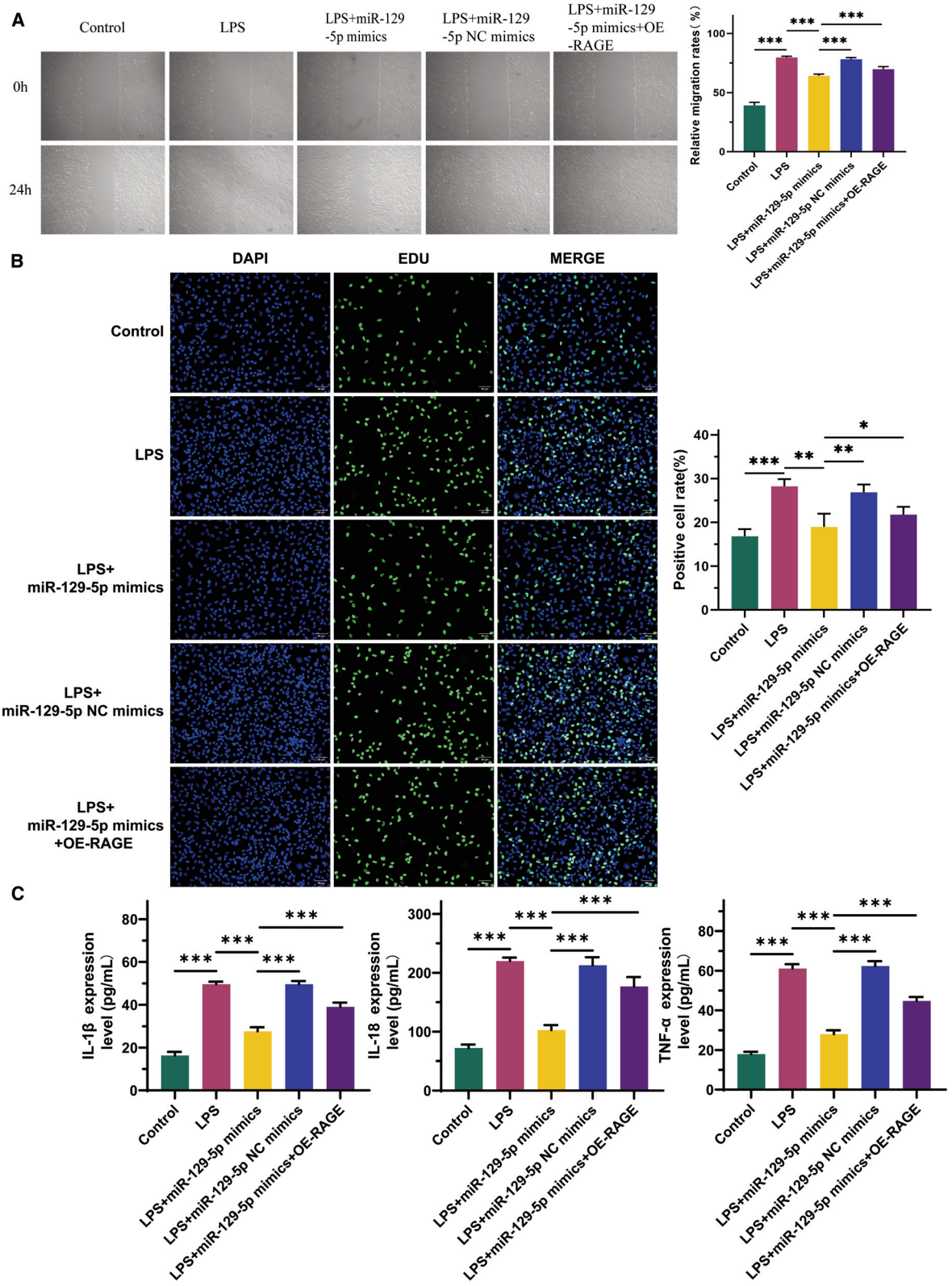

Figure 5. miR-129-5p regulates the HMGB1/RAGE axis to ameliorate LPS-mediated deterioration of cervical epithelial cells. **A**) The scratch wound healing assay was performed to evaluate the migration ability of cervical epithelial cells under different treatment conditions, including control (untreated), LPS treatment alone, LPS + miR-129-5p mimics, and LPS + miR-129-5p mimics + OE-RAGE. Representative images at 0 h and 24 h post-scratch are shown, reflecting the wound closure process in each group. **B**) The EdU incorporation assay was conducted to assess the proliferation ability of cervical epithelial cells under the same treatment conditions as described in (**A**); representative images of DAPI and EdU staining are shown, along with merged images; quantification of positive cell rates is also provided. **C**) ELISA was performed to measure the levels of pro-inflammatory cytokines IL-1β, IL-18, and TNF-α in the supernatants of cervical epithelial cells under the same treatment conditions as described in panels (**A,B**). n=3, *p<0.05, **p<0.01, ***p<0.001.

demonstrated that miR-129-5p can inhibit pyroptosis by targeting the HMGB1/RAGE axis, thereby improving the deterioration of cervical epithelial cells. This discovery revealed for the first time the protective role of miR-129-5p in CC cells. Specifically, overexpression of miR-129-5p significantly downregulated HMGB1 expression levels, thereby suppressed RAGE activation and ultimately decreased the production of pyroptosis markers such as Gasdermin D cleavage fragments. These findings not only underscore the regulatory role of miR-129-5p in cancer progression but also highlight its therapeutic potential in CC.

HMGB1, a nuclear protein, functions not only in gene expression regulation but also as a damage-associated molecular pattern molecule that exerts extracellular effects.[22] HMGB1 binds to its receptor RAGE, activating multiple downstream signaling pathways such as NF-κB and MAPK pathways, thereby promoting cellular inflammation and pyroptosis.[23] In CC, activation of the HMGB1/RAGE axis is considered a critical mechanism for cellular deterioration and cancer progression.[15] Previous studies have shown that the HMGB1/RAGE axis plays a crucial role in the development of various cancers, closely linked with pyroptosis.[14] Our study demonstrated that stimulation by LPS significantly activated the HMGB1/RAGE axis, thereby induced pyroptosis in cervical epithelial cells. Inhibition of HMGB1/RAGE axis activation significantly attenuated LPS-induced pyroptosis, thereby ameliorating the deterioration of cervical epithelial cells. Our research revealed the role of the HMGB1/RAGE axis in inducing pyroptosis in the deterioration of cervical epithelial cells, further expanding our understanding of this signaling pathway.

Pyroptosis is a form of programmed cell death mediated by inflammasomes, characterized by significant inflammatory features.[24] Pyroptosis activates Caspase-1 and promotes GSDMD cleavage, forming pore structures that lead to cell membrane rupture and release of cellular contents, triggering intense inflammatory responses.[25] In CC, pyroptosis is considered a critical mechanism for cellular deterioration and cancer progression.[26] Current research has indicated that pyroptosis played a crucial role in the development of various cancers through its unique inflammatory response mechanisms.[25] Our results demonstrated that LPS can induce pyroptosis in cervical epithelial cells by activating the HMGB1/RAGE axis, exacerbated cellular deterioration. However, overexpression of miR-129-5p significantly inhibited this process, protected cervical epithelial cells. Our study further validated the role of pyroptosis in the deterioration of CC cells, supporting its potential as a therapeutic target in cancer treatment.

Through a series of experiments, we verified the functional relationship between miR-129-5p, the HMGB1/RAGE axis, and pyroptosis. First, RT-qPCR and Western blot analyses showed that miR-129-5p overexpression significantly reduced both HMGB1 mRNA and protein expression levels, as well as inhibited RAGE activation. Second, by detecting pyroptosis markers such as GSDMD-N, we observed that miR-129-5p overexpression markedly suppressed LPS-induced GSDMD-N production, indicating that miR-129-5p effectively inhibits LPS-induced pyroptosis. Collectively, these results demonstrated that miR-129-5p suppresses pyroptosis by targeting HMGB1, thereby inhibiting RAGE activation and downstream pyroptotic signaling, ultimately ameliorating the deterioration of cervical epithelial cells. Our study systematically validated the protective role of miR-129-5p in cervical epithelial cell injury, filling an important research gap in this field.

Despite clarifying the pivotal role of miR-129-5p in CC pathogenesis, unresolved questions persist concerning its interaction with auxiliary signaling pathways, mechanistic heterogeneity among molecular subtypes, and clinical applicability demanding thorough preclinical and clinical validation. From a translational standpoint, miRNAs such as miR-129-5p show strong potential as non-invasive biomarkers and therapeutic targets in precision oncology due to their stability in biofluids and regulatory roles in oncogenic pathways. However, their clinical integration requires rigorous validation, along with careful consideration of ethical, legal, and regulatory frameworks to ensure safe and effective implementation in personalized cancer care.[27-30] Consequently, future investigations must prioritize evaluating therapeutic potential through *in vivo* models, formulating subtype-specific targeting approaches, conducting human trials for efficacy and safety assessment, and applying CRISPR-Cas9-based precision editing technology. In conclusion, our systematic experimental investigation demonstrated that miR-129-5p exerted a protective effect against cervical epithelial cell deterioration by suppressing pyroptosis through regulating the HMGB1/RAGE axis *in vitro*. These findings not only advanced our understanding of CC pathogenesis but also provided novel therapeutic insights for potential clinical interventions. Future studies will further elucidate the mechanistic actions of miR-129-5p and evaluate its translational potential, ultimately contributing to improved treatment strategies for CC patients.

Acknowledgments

The authors express their appreciation to all the staff involved in this study.

References

1. Cohen PA, Jhingran A, Oaknin A, Denny L. Cervical cancer. Lancet 2019;393:169-82.
2. Ngcobo N, Jaca A, Iwu-Jaja CJ, Mavundza E. Reflection: burden of cervical cancer in Sub-Saharan Africa and progress with HPV vaccination. Curr Opin Immunol 2021;71:21-6.
3. Luo QQ, Tian Y, Qu GJ, Kun-Huang, Luo SS. Functional mechanism and clinical implications of miR-141 in human cancers. Cell Signal 2022;95:110354.
4. Margaritis K, Margioula-Siarkou G, Giza S, Kotanidou EP, Tsinopoulou VR, Christoforidis A, et al. Micro-RNA Implications in type-1 diabetes mellitus: a review of literature. Int J Mol Sci 2021;22:12165.
5. Zhao G. Significance of non-coding circular RNAs and micro RNAs in the pathogenesis of cardiovascular diseases. J Med Genet 2018;55:713-20.
6. Budakoti M, Panwar AS, Molpa D, Singh RK, Busselberg D, Mishra AP, et al. Micro-RNA: The darkhorse of cancer. Cell Signal 2021;83:109995.
7. Motshwari DD, Matshazi DM, Erasmus RT, Kengne AP, Matsha TE, George C. MicroRNAs associated with chronic kidney disease in the general population and high-risk subgroups - A systematic review. Int J Mol Sci 2023;24:1792.
8. Tornesello ML, Faraonio R, Buonaguro L, Annunziata C, Starita N, Cerasuolo A, et al. The role of microRNAs, long non-coding RNAs, and circular RNAs in cervical cancer. Front Oncol 2020;10:150.
9. Wang YF, Yang HY, Shi XQ, Wang Y. Upregulation of microRNA-129-5p inhibits cell invasion, migration and tumor angiogenesis by inhibiting ZIC2 via downregulation of the Hedgehog signaling pathway in cervical cancer. Cancer Biol Ther 2018;19(12):1162–73.
10. Wang YF, Yang HY, Shi XQ, Wang Y. Upregulation of microRNA-129-5p inhibits cell invasion, migration and tumor

angiogenesis by inhibiting ZIC2 via downregulation of the Hedgehog signaling pathway in cervical cancer. Cancer Biol Ther 2018;19:1162-73.
11. Feng J, Guo J, Wang JP, Chai BF. MiR-129-5p inhibits proliferation of gastric cancer cells through targeted inhibition on HMGB1 expression. Eur Rev Med Pharmaco 2020;24:3665-73.
12. Sims GP, Rowe DC, Rietdijk ST, et al. HMGB1 and RAGE in inflammation and cancer. Annu Rev Immunol 2010;28:367–88.
13. Pickering RJ, Tikellis C, Rosado CJ, et al. Transactivation of RAGE mediates angiotensin-induced inflammation and atherogenesis. J Clin Invest 2019;129:406–21.
14. Gao T, Huang Z. Effects of Isoflurane on the cell pyroptosis in the lung cancer through the HMGB1/RAGE pathway. Appl Biochem Biotech 2024;196:3786-99.
15. You L, Cui H, Zhao F, Sun H, Zhong H, Zhou G, et al. Inhibition of HMGB1/RAGE axis suppressed the lipopolysaccharide (LPS)-induced vicious transformation of cervical epithelial cells. Bioengineered 2021;12:4995-5003.
16. Wang RT, Zhang Y, Yao SY, Tan XG. LINC00501 inhibits the growth and metastasis of lung cancer by mediating miR-129-5p/HMGB1. Oncotargets Ther 2020;13:7137-49.
17. Gu LP, Jin S, Xu RC, Zhang J, Geng YC, Shao XY, et al. Long non-coding RNA PCAT-1 promotes tumor progression by inhibiting miR-129-5p in human ovarian cancer. Arch Med Sci 2019;15:513-21.
18. Yao N, Fu Y, Chen L, Liu Z, He J, Zhu Y, et al. Long non-coding RNA NONHSAT101069 promotes epirubicin resistance, migration, and invasion of breast cancer cells through NONHSAT101069/miR-129-5p/Twist1 axis. Oncogene 2019;38:7216-33.
19. Luo W, Wang J, Xu W, Ma C, Wan F, Huang Y, et al. LncRNA RP11-89 facilitates tumorigenesis and ferroptosis resistance through PROM2-activated iron export by sponging miR-129-5p in bladder cancer. Cell Death Dis 2021;12:1043.
20. Sun N, Zhang W, Liu J, Yang X, Chu Q. Propofol inhibits the progression of cervical cancer by regulating HOTAIR/miR-129-5p/RPL14 axis. Oncotargets Ther 2021;14:551-64.
21. Han C, Wang W. MicroRNA-129-5p suppresses cell proliferation, migration and invasion via targeting ROCK1 in osteosarcoma. Mol Med Rep 2018;17:4777-84.
22. Wang S, Zhang Y. HMGB1 in inflammation and cancer. J Hematol Oncol 2020;13:116.
23. Gao J, Zhang Z, Yan JY, Ge YX, Gao Y. Inflammation and coagulation abnormalities via the activation of the HMGB1−RAGE/NF−kappaB and F2/Rho pathways in lung injury induced by acute hypoxia. Int J Mol Med 2023;52:67.
24. Hsu SK, Li CY, Lin IL, Syue WJ, Chen YF, Cheng KC, et al. Inflammation-related pyroptosis, a novel programmed cell death pathway, and its crosstalk with immune therapy in cancer treatment. Theranostics 2021;11:8813-35.
25. Rao Z, Zhu Y, Yang P, Chen Z, Xia Y, Qiao C, et al. Pyroptosis in inflammatory diseases and cancer. Theranostics 2022; 12:4310-29.
26. Li K, Qiu J, Pan J, Pan JP. Pyroptosis and its role in cervical cancer. Cancers 2022;14:5764.
27. Passaro A, Al Bakir M, Hamilton EG, Diehn M, André F, Roy-Chowdhuri S, et al. Cancer biomarkers: Emerging trends and clinical implications for personalized treatment. Cell 2024;187:1617-35.
28. Gulìa C, Signore F, Gaffi M, Gigli S, Votino R, Nucciotti R, Bertacca L, et al. Y RNA: An overview of their role as potential biomarkers and molecular targets in human cancers. Cancers (Basel) 2020;12:1238.
29. Piergentili R, Del Rio A, Signore F, Umani Ronchi F, Marinelli E, Zaami S. CRISPR-Cas and its wide-ranging applications: From human genome editing to environmental implications, technical limitations, hazards and bioethical issues. Cells 2021;10:969.
30. Ramaswami R, Bayer R, Galea S. Precision medicine from a public health perspective. Annu Rev Public Health 2018;39:153-68.

Received: 20 May 2025. Accepted: 11 August 2025.

European Journal of Histochemistry 2025; 69:4238
doi:10.4081/ejh.2025.4238